Journal of Institute of Science and Technology, 29(1), 1-11 (2024)
ISSN: 2467-9062 (print), e-ISSN: 2467-9240
https://doi.org/10.3126/jist.v29i1.60793

Research Article

IN-SITU ASSESSMENT OF NATURAL RADIOACTIVITY CONCENTRATIONS AND HAZARD INDICATORS IN THE MINING AREA OF LALITPUR, NEPAL

Devendra Raj Upadhyay[1,2*], Pramod Adhikari[3], Bal Vikram Khatri[1,2], Suffian Mohamad Tajudin[4], Himali Kalakhety[5], Raju Khanal[1]

[1]*Central Department of Physics, Institute of Science and Technology, Tribhuvan University, Kirtipur, Nepal.*
[2]*Department of Physics, Amrit Campus, Tribhuvan University, Thamel, Nepal.*
[3]*Department of Physics, Patan Multiple Campus, Tribhuvan University, Lalitpur, Nepal.*
[4]*Faculty of Health Sciences, Sultan Zainal Abidin University, Terengganu, Malaysia.*
[5]*Department of Physics and Geosciences, Texas A & M University, Kingsville, Texas, USA.*
**Correspondence: devendra.upadhyay@ac.tu.edu.np*

(***Received***: *December 17, 2023;* ***Final Revision***: *January 10, 2024;* ***Accepted***: *March 17, 2024)*

ABSTRACT

Urban construction materials predominantly originate from mining sites, raising concerns about the associated natural radioactivity and its potential health impacts. This work focuses on assessing the distribution of three natural radionuclides and associated radiological indicators in the South Lalitpur mining area in Nepal. A portable gamma spectrometer information system (PGIS-2) was employed for in-situ measurement of natural radionuclide concentrations. The mean activity concentrations of ^{238}U, ^{232}Th, and ^{40}K were found to be 85.82 ± 40.63 Bq kg^{-1}, 104.87 ± 30.42 Bq kg^{-1}, and 1257.47 ± 304.36 Bq kg^{-1}, respectively. Radiological hazard parameters were computed and compared with global averages, revealing a radium equivalent activity (Ra_{eq}) mean of 332.62 ± 63.08 Bq kg^{-1}, slightly below the global average. The average absorbed gamma radiation dose rate in the air was 155.94 ± 29.09 nSv hr^{-1}, over twice the world average. Indoor and outdoor annual effective dose rates, excess lifetime cancer risks, and annual gonadal dose equivalents were slightly higher than world averages. Additional radiological indices were computed, indicating that most estimated parameters exceeded global averages. Multivariate statistical analysis was applied to the dataset. The study suggests that in-situ measurements of these radiological parameters in mining areas are essential, as most mean values were above global averages, emphasizing the need for environmental safety and awareness in mining regions.

Keywords: Hazards, in-situ spectroscopy, mining area, NORMs, statistics

INTRODUCTION

Radionuclides are unstable forms of chemical elements that undergo radioactive decay, emitting nuclear radiation. Among the various pathways through which humans can be exposed to ionizing radiation, the uptake of radionuclides by agricultural plants intended for human consumption is a critically important route. Radionuclides can be categorized into different types, including cosmogenic radionuclides (e.g., ^{3}H, ^{7}Be, ^{11}C, ^{14}C, ^{22}Na) (Galbiati *et al.*, 2005) and terrestrial radionuclides (e.g., ^{238}U, ^{235}U, ^{232}Th, and ^{40}K), which contribute to human exposure in our surroundings (García-León, 2023). With over 256 known stable nuclides, systems lacking stable configurations undergo spontaneous radioactive decay until they attain stability. If the half-life of such an unstable nuclideis significantly longer than 10^{-21} seconds, a typical timescale for processes governed by the strong interaction,the nucleus is considered a well-defined entity (Pfützner *et al.*, 2012). The importance of instant measurements is steadily increasing due to various environmental challenges we encounter daily. Such measurements of naturally occurring radioactive materials (NORMs) provide insight into the concentration of ^{226}Ra, ^{238}U, ^{232}Th, and ^{40}K. In today's context, in-situ measurements of environmental radioactivity are crucial for understanding the instantaneous situation of NORMs activity. Several authors have reported their findings using in-situ measurements of environmental radionuclides, accompanied by hazard indices at Kwara and southwestern Nigeria (Joel *et al.*, 2021; Usikalu *et al.*, 2022), mining sites in Nigeria (Orosun *et al.*, 2021), south coastal region of Kenya (Kaniu *et al.*, 2018b,1) and Mrima-Kiruku complex, Kenya (Kaniu *et al.*, 2018a) using RS-125 and PGIS-2 handheld gamma ray spectrometer. However, limited research has focused on ground-based in-situ gamma radiation rates and ambient radioactivity in Nepal, with only a few studies addressing these aspects at Lower and Upper Mustang, Gorang and Bagabagar Baitadi, Tin Bhangale Makawanpur (Khadka & Maharjan, 2019), Shivapuri Area Kathmandu (Khadka & Lamsal, 2020) and Ampipal, Daraudi Kh, Ghyampesal, Jaubari, Gyazi Gorkha area (Khadka & Lamsal, 2022) they found relatively high activity region at those place. Similarly, premises of Tribhuvan University (Mishra & Khanal, 2019), UNESCO World Heritage Sites in Kathmandu Valley (Mishra & Khanal, 2023b), Hetauda City (Mishra & Khanal, 2023a). In this study, we present a systematic survey of radionuclides such as ^{238}U, ^{232}Th, and ^{40}K in the environment of a mining area in Lalitpur district, Nepal from where a

majority of construction materials is regularly imported to highly populated cities like Kathmandu, Lalitpur, and Bhaktapur districts in Nepal. We employ a portable gamma-ray spectrometer system (PGIS-2) for this investigation. The primary objective of this study is to evaluate radiological concentrations and estimate corresponding hazard indices, including radium equivalent index, absorbed dose rate, outdoor annual effective dose equivalent, outdoor excess lifetime cancer risk, annual gonadal dose equivalent, internal hazard index, external hazard index, gamma index, alpha index, representative level index, and activity utilization index at the mining area in Lalitpur. In the present context of Nepal, this work based on in-situ measurements using PGIS-2 may serve as a crucial step toward assessing environmental radioactivity concentrations in real-time and for establishing national guidelines and regulations regarding environmental radiation safety.

MATERIALS AND METHODS

Study Area

The mining area is located in the Godawari Municipality ward no. 6 Lele, Lalitpur district of Bagmati province, Nepal. The survey region lies at an altitude from 1503.20 to 1618.20 meters above sea level. Fig. 1 represents the geological map of Nepal, and the arrow pointing circle represents the map of the Godawari Municipality where our study is based. The figure at the top left in the local map represents the mining area and location spot. All locations of the survey region are shown in Fig. 1.

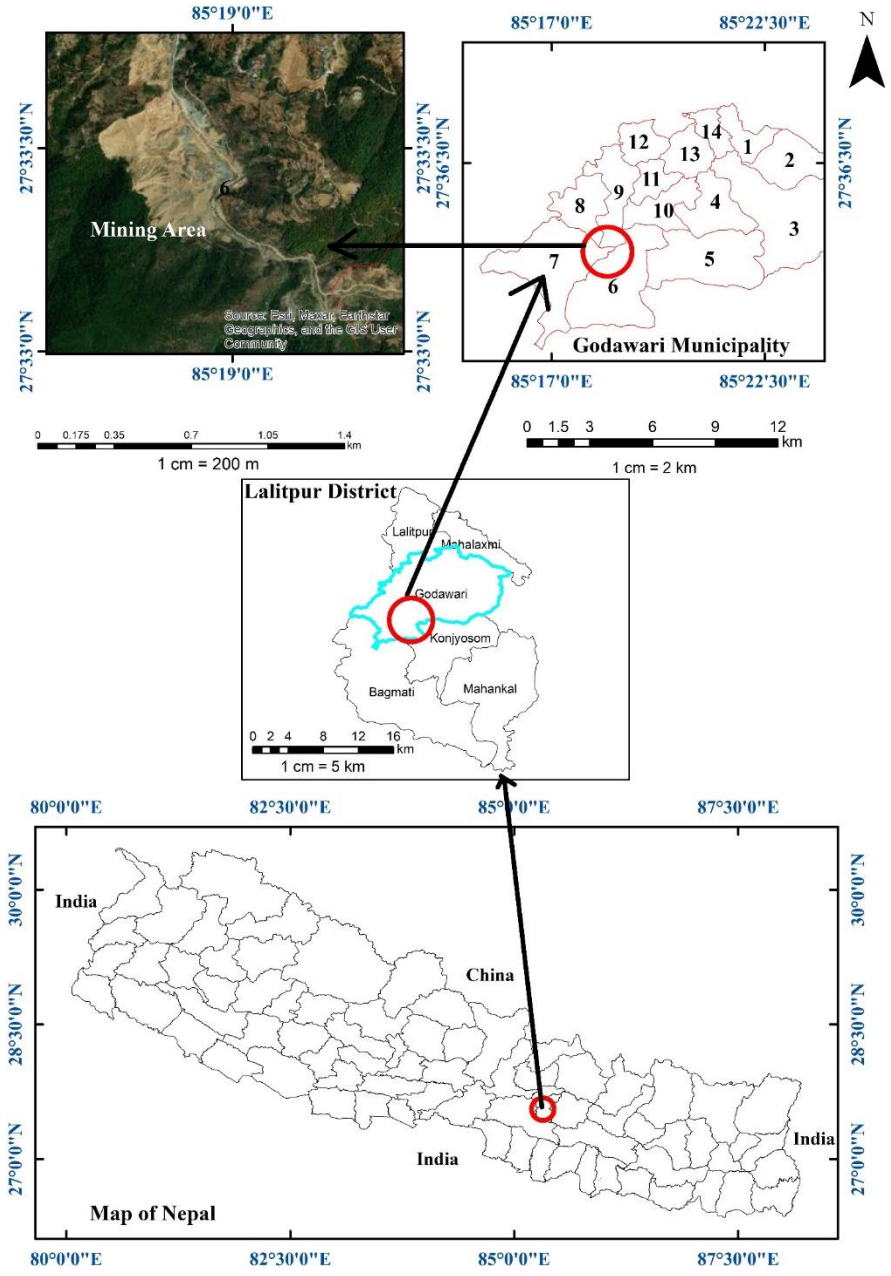

Figure 1. Map representing survey locations of study region at Mining area Lalitpur

We have selected a mining area as our study area, as this region serves as a primary source of construction materials, including soils, rocks, gravels, and even water, that are regularly imported to densely populated cities. The impact of these materials on public health can be direct or indirect. The rationale behind choosing a mining area lies in the fact that since a significant portion of construction materials originates from mining areas, there is a higher likelihood of elevated concentrations of radionuclides such as ^{238}U, ^{232}Th, and ^{40}K.

Instrumentation

The detector is equipped with thallium-activated sodium iodide, NaI(Tl) crystal of volume 0.347 L. The energy resolution of this detector was 661.6 keV (^{137}Cs). The spectrometer consists of a scintillation detector unit integrated with Global Positioning System (GPS) and a data logger unit (developed for Android mobile). The detector has wireless communication with the data logger unit via Bluetooth and provides real-time navigation guidance to the operator. The detector is coupled with a multichannel analyzer (MCA) of 512 channels and the energy range of the detector is 20 keV to 3 MeV. It can measure per second spectra and its startup stabilization (tuning) time is less than a minute. The GPS connection to the data stream via Bluetooth connection to the device is used to determine the position of the data. The radionuclides Potassium: ^{40}K in percentage (pct), Uranium: ^{238}U, and Thorium: ^{232}Th in parts per million (ppm) are immediately can record and transferred by the PGIS-2 to the mobile via Bluetooth, which also analyzes sample concentration. For the best analysis, it also offers a user-selectable sample time. The utility program that comes with the PGIS-2 is used to download the memory-stored data. Through Bluetooth or USB, the PGIS-2 device's memory may be completely transferred to a personal computer. The instrument is auto calibrated and granted by IAEA TC Project NEP002. To consistency and accuracy in calculating potassium, uranium, and thorium, the portable equipment was calibrated. The rate of exposure or dosage absorbed through the use of conversion factors emerging from this radiation might be used to indicate the effect of this radiation in the atmosphere. Readings were taken using a radiation detector PGIS 2 as shown in Fig. 2 at mining area, with the detector being held 1 meter above the ground as a similar method obeyed by Joel *et al.* (2021), Mishra and Khanal, (2023a) and several authors (Adewoyin *et al.*, 2022; Kaniu *et al.*, 2019). The readings were measured in ppm, and pct, and the results were converted to Becquerel per kilogram (Bq kg^{-1}) using some standard conversion factor.

Theoretical Background

We obtained values of ^{238}U, ^{232}Th and ^{40}K concentrations in terms of parts per million (ppm) and percentage (%) using PGIS-2. Where, 1 parts per million (ppm) ^{238}U shows 12.35 Bq kg^{-1} activity, similarly 1 ppm ^{232}Th is equivalent to 4.06 Bq kg^{-1} and 1% ^{40}K equivalent to 313 Bq kg^{-1} as mentioned in (Joel *et al.*, 2021; UNSCEAR, 2000). Those values recommend by (UNSCEAR, 2000) ≤33 for ^{238}U, ≤45 for ^{232}Th ≤420 for ^{40}K. The radiological parameters were determined using empirical formula reported by (UNSCEAR, 2000) and used by various researchers (Inoue *et al.*, 2020; Liu & Lin, 2018; UNSCEAR, 2000).

Figure 2. Portable Gamma spectrometer Information System (PGIS 2)

Calculation of Hazard Indices

Radium equivalent index (Ra_{eq}) describes the combined activity of terrestrial radionuclei ^{238}U, ^{232}Th and ^{40}K. Here the factor indicates the compensating factors. According to UNSCEAR (2000) report its values ≤ 370 Bq kg^{-1} in the environment or public places (Joel *et al.*, 2021; UNSCEAR, 2000). The empirical formula presented as Eq. (1)

$$Ra_{eq} = A_U + 1.43A_{Th} + 0.077A_K \quad (1)$$

The internal and external hazard index are a measure that takes into account the activities of different radionuclides (uranium, thorium, and potassium) and combines them using specific weighting factors (the constants in the denominators). The purpose is to evaluate the potential internal hazards associated with exposure inside and outside the building or constricted place to these radionuclides presented as empirical formula Eq. (2) and Eq. (3) (Joel *et al.*, 2021).

$$H_{in} = \frac{A_U}{185} + \frac{A_{Th}}{259} + \frac{A_K}{4810} \quad (2)$$

and $$H_{ex} = \frac{A_U}{370} + \frac{A_{Th}}{259} + \frac{A_K}{4810} \quad (3)$$

Similarly, gamma index (I_γ) and alpha index (I_α) are associated with the hazard linked to the excess external gamma radiation and alpha particles induced by superficial substances are represented by Eq. (4) and Eq. (5) (Joel *et al.*, 2021; Ravisankar *et al.*, 2014):

$$I_\gamma = \frac{A_U}{300} + \frac{A_{Th}}{200} + \frac{A_K}{3000} \quad (4)$$

and $$I_\alpha = \frac{A_U}{200} \quad (5)$$

Additionally, the dose received per hour from radionuclei expressed as dose rate in nSv hr^{-1} and represented as Eq. (6) (5) (Joel *et al.*, 2021; Ravisankar *et al.*, 2014):

$$D_R = 0.43A_U + 0.623A_{Th} + 0.0427A_K \quad (6)$$

The annual effective dose rate in mSv yr^{-1} received from

materials inside ($AEDE_{in}$) and outside ($AEDE_{out}$) the building materials constructed form raw materials can be expressed as Eq. (7) and Eq. (8) (Attallah *et al.*, 2020; Ravisankar *et al.*, 2014):

$$AEDE_{in} = D_R \times 8760\ (hr^{-1}) \times 0.7\ (Sv\ Gy^{-1}) \times 0.8 \times 10^{-6} \quad (7)$$

Where D_R represents the gamma absorbed dose rate (GADR), with occupancy factors of 0.8 and 0.2, a conversion coefficient of 0.7, and a time of 8760 hours for a span of 365 days (Belyaeva *et al.*, 2021; Suresh *et al.*, 2022).

$$AEDE_{out} = D_R \times 8760\ (hr^{-1}) \times 0.7(Sv\ Gy^{-1}) \times 0.2 \times 10^{-6} \quad (8)$$

Also another hazard indicator excess lifetime cancer risk inside ($ELCR_{in}$) and outside ($ELCR_{in}$) expressed as in Eq. (10) and Eq. (11) (Suresh *et al.*, 2022):

$$ELCR_{in} = AEDE_{in} \times DL \times RF \quad (9)$$

$$\text{and } ELCR_{out} = AEDE_{out} \times DL \times RF \quad (10)$$

Where, factors DL and RF correspond to the duration of life (70 years) and risk factor (Sv^{-1}), which indicates the fatal cancer risk per Sievert. ICRP 60 guidelines consider a value of 0.05 for the public when addressing stochastic effects (Belyaeva *et al.*, 2021; ICRP, 1991).

$$AGDE = 3.09A_U + 4.18A_{Th} + 0.214A_K \quad (11)$$

Representative Level Index is the level of gamma radioactivity associated with different concentrations of certain specific radionuclides and expressed as in Eq. (12) (Attallah *et al.*, 2020; Sam & Abbas, 2001)

$$RLI = \frac{A_U}{150} + \frac{A_{Th}}{100} + \frac{A_K}{1500} \quad (12)$$

and to simplify the computation of dose rates in air arising from various combinations of the three radionuclides in building/construction materials, and by employing the relevant conversion factors, an Activity Utilization Index (AUI) can be formulated, as indicated by Eq. (13) (Ravisankar *et al.*, 2014)

$$AUI = \frac{A_U}{50} f_U + \frac{A_{Th}}{50} f_{Th} + \frac{A_K}{500} f_K \quad (13)$$

Where, the activity concentrations of ^{238}U, ^{232}Th, and ^{40}K, denoted as A_U, A_{Th}, and A_K respectively, are measured in units of Bq kg^{-1}. The fractional contributions to the total dose rate resulting from radiation emitted by ^{226}Ra, ^{232}Th, and ^{40}K are represented as f_U (0.462), f_{Th} (0.604), and f_K (0.042) respectively (Ravisankar *et al.*, 2014). All recommended limits of parameters are presented in Table 3 and Table 4 (UNSCEAR, 2000).

Data Analysis

The analysis of the results involved utilizing LibreOffice Calculator, Python 3 and ArcMap. The Pearson correlation coefficients were computed to examine the relationships between variables as done by (Ravisankar *et al.*, 2014), and (Tchorz-Trzeciakiewicz *et al.*, 2023). Furthermore, statistics such as minimum, maximum, Range (R), quartiles (Q_1, Q_2, and Q_3), interquartile range (IQR), mean, geometric mean (GM), standard deviation (S.D.), Coefficient of variation (C.V.), variance, Median Absolute Deviation (MAD), Skewness (S_K) and Kurtosis (K) are analyzed using Python programming as presented by (Ravisankar *et al.*, 2014; Ghias *et al.*, 2021).

RESULTS AND DISCUSSION

Altogether 10433 data were recorded by using PGIS-2 related to naturally occurring radionuclides concentration consisting of activity in ppm and pct. Table 1 presents the statistical analysis of reduced data using several empirical formulas as mentioned in Table 2. Here, the first column represents the statistical parameters mean, S.D. minimum, first quartile, median, third quartile, maximum value, range, skewness, kurtosis, variance, MAD, CV, and obtained mean values were compared with UNSCEAR 2000 report mentioned values (UNSCEAR, 2000). Similarly, the second, third, fourth, and fifth column shows those statistically calculated values corresponding to activity concentration of uranium, thorium, potassium, and radium equivalent activity respectively. From the analysis, it was determined that the mean values for activity concentration in the region of the study were ordered as follows: and ^{40}K (1257.47 Bq kg^{-1}) > ^{232}Th (104.87 Bq kg^{-1}) > ^{238}U (85.82 Bq kg^{-1}). The value of standard deviation or uncertainties in measurements is high due to the fact that we didn't repeat data recording at a place we took recording by walk at most of the mining area at which stone mining was ongoing. Every location has a different chemical composition of rocks, so it has a higher S.D. value which is an expected value in terms of statistical analysis.

A skewness value between -3 and 3 covers the range of approximately 99.73% of the data distribution while a skewness value between -2 and 2 covers the range of approximately 95.45% of the data distribution. However, our study reveals that the skewness range of (-1 < skewness 1) covers the range of approximately 68.27% of the data distribution. This range indicates a distribution that is relatively close to being symmetric or mildly skewed. The skewness value of concentrations of radionuclides was found to be ^{238}U (-1<0.604< 1), ^{232}Th (-1 <0.29< 1), and ^{40}K (-1 <-0.17< 1) which are in the descending order. A skewness value of 0.604 indicates a moderate rightward (positive) skew in the data distribution, suggesting that there are slightly larger values on the right side of the distribution of ^{238}U. However, the distribution of ^{40}K concentrations shows normal distribution. Whereas the distribution of ^{232}Th concentrations shows inter-mediated distribution between

^{238}U and ^{40}K. In Fig. 3(a), (b) and (c) means (μ), standard deviation (σ), number of data (N), and bins size are presented in each figure. Also, we obtained a kurtosis value positive (>0) which indicates that the distribution has heavier tails and is more "peaked" around the mean compared to a normal distribution which is called leptokurtic.

It suggests that there are more extreme values present in the data compared to a normal distribution. Similarly, we have estimated quartiles, variance, mean absolute deviation (MAD), coefficient of variance of radiological concentration and hazard indices and calculated mean values which has been compared with UNSCEAR reported world average value as shown in Table 1 and Table 2.

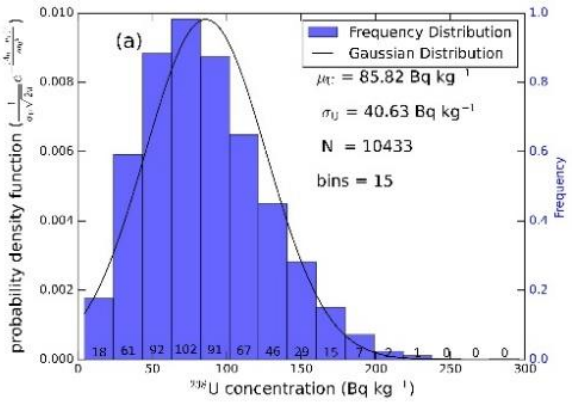

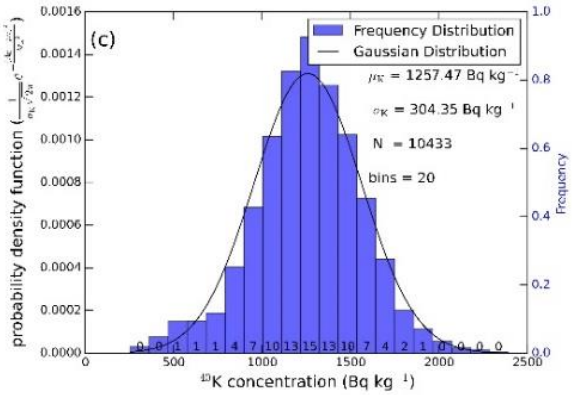

Figure 3. Frequency and probability density function distribution of ^{238}U (a), ^{232}Th (b), and ^{40}K (c)

As statistical analysis Pearson correlation coefficients were calculated between all parameters, and standard deviation (S.D.), minimum, first quartile, median, third quartile, maximum value, range, variance, MAD, and CV. Similarly, Table 2 shows statistical analyzed values of annual gonadal dose equivalent, internal and external hazard indices, gamma index, alpha index, representative level index and activity utilization index. Fig. 4 (a) shows a diagram of Ra_{eq} against ^{238}U concentration at mining area. Linear fitting shows poor correlation between those parameters with Pearson correlation coefficient (r = 0.49) with mean ± S.D. value of ^{238}U concentration 85.82 Bq kg^{-1} ± 40.63 Bq kg^{-1}. Whereas that of Ra_{eq} value is 332.62 ±63.08 Bq kg^{-1}. The best-fitted line we obtained is as follows:

$$Ra_{eq} = 0.75^{238}U + 267.70 \qquad (14)$$

Where the values of slope and intercept are 0.75 and 267.70 Bq kg^{-1} respectively as demonstrated in Fig. 4 (a). Fig. 4 (b) shows a correlation between Ra_{eq} against ^{232}Th concentration at mining area. It shows a correlation between those parameters with Pearson correlation coefficient (r = 0.68) with mean ± S.D. value of ^{232}Th concentration 104.87 Bq kg^{-1} ±30.42 Bq kg^{-1}.

$$Ra_{eq} = 1.41\ ^{232}Th + 184.61 \qquad (15)$$

Table 1. Statistical analysis of radionuclides concentration and hazard indices

Particulars	A_U (Bq kg^{-1})	A_{Th} (Bq kg^{-1})	A_K (Bq kg^{-1})	Ra_{eq} (Bq kg^{-1})	D_R (nSv hr^{-1})	$AEDR_O$ (mSv yr^{-1})	$AEDR_I$ (mSv yr^{-1})	$ELCR_O$ ×10^{-3}	$ELCR_I$ ×10^{-3}
N	10433	10433	10433	10433	10433	10433	10433	10433	10433
Mean	85.82	104.87	1257.47	332.62	155.94	0.19	0.69	0.67	2.34
S.D.	40.63	30.42	304.37	63.08	29.09	0.04	0.13	0.13	0.44
Min	4.57	11.64	255.10	104.42	50.39	0.06	0.22	0.22	0.76
Q_1	55.46	83.88	1075.78	298.22	140.29	0.17	0.60	0.60	2.11
Median	80.82	103.43	1264.21	333.61	156.45	0.19	0.67	0.67	2.35
Q_3	111.11	124.16	1453.57	369.70	173.04	0.21	0.74	0.74	2.60
Max	295.87	250.78	2390.07	612.72	282.73	0.35	1.21	1.21	4.25
Range	291.30	239.14	2134.97	508.29	232.35	0.29	0.99	0.99	3.49
Skewness	0.60	0.29	-0.17	-0.27	-0.33	-0.33	-0.33	-0.33	-0.33
Kurtosis	0.18	0.19	0.52	1.35	1.51	1.51	1.51	1.51	1.51
Variance	1650.95	925.56	92640.68	3979.07	846.27	1.00×10^{-3}	0.02	0.02	0.19
MAD	32.65	24.09	235.22	46.97	21.53	2.60×10^{-3}	0.09	0.09	0.32
CV	47.34	29.01	24.21	18.97	18.66	18.66	18.66	18.66	18.66
(UNSCEAR, 2000)	33	45	420	370	59	0.07	0.26	0.26	0.90

Table 2. Descriptive statistical analysis of radionuclides and hazard indices

Particulars	*AGDE* (μSv hr^{-1})	H_{in}	H_{ex}	I_γ	I_α	*RLI*	*AUI*
N	10433	10433	10433	10433	10433	10433	10433
Mean	972.67	1.13	0.90	1.23	0.43	2.46	2.17
S.D.	185.88	0.24	0.17	0.23	0.20	0.45	0.47
Min	302.65	0.34	0.28	0.40	0.02	0.80	0.56
Q_1	869.87	0.98	0.81	1.11	0.28	2.21	1.87
Median	975.30	1.12	0.90	1.23	0.40	2.47	2.16
Q_3	1081.85	1.28	0.99	1.37	0.56	2.73	2.46
Max	1808.69	2.29	1.66	2.23	1.48	4.45	4.30
Range	1506.04	1.95	1.37	1.83	1.46	1.00×10^{-3}	3.76
Skewness	-0.24	0.09	-0.27	-0.33	0.60	-0.33	0.06
Kurtosis	1.30	0.85	1.35	1.50	0.18	1.49	0.60
Variance	34550.79	0.06	0.03	0.05	0.04	0.21	0.23
MAD	138.75	0.19	0.13	0.17	0.16	0.34	0.37
CV	19.11	21.55	18.97	18.66	47.34	18.67	21.89
(UNSCEAR, 2000)	300	1	1	1	1	1	2

Where the values of slope and intercept are 1.41 and 184.61 Bq kg^{-1} respectively as shown in Eq. (15). The correlation between Ra_{eq} and ^{40}K concentration in an environment of the mining area is shown in Fig. 4(c). It shows a correlation between Ra_{eq} against ^{40}K as Pearson correlation coefficient is 0.58 with mean ± S.D. value of ^{40}K concentration 1257.47 Bq kg^{-1} ± 304.37 Bq kg^{-1}.

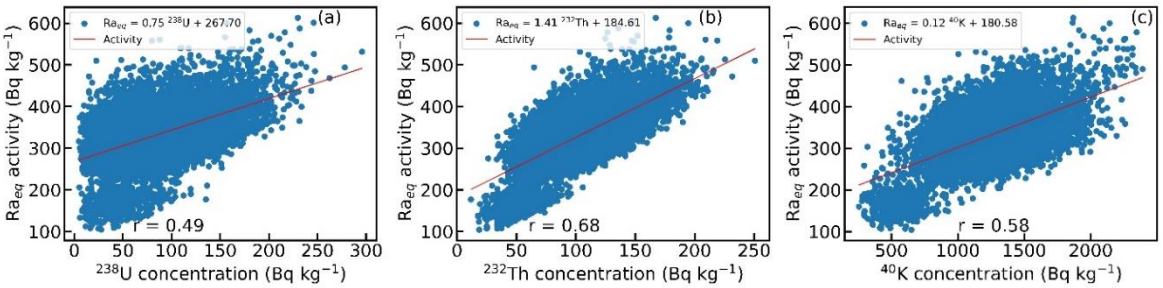

Figure 4. Correlation between activity concentration of ^{238}U (a), ^{232}Th (b), ^{40}K (c) and radium equivalent

Figures 4(a), 4(b), and 4(c) show how terrestrial radionuclei concentrations affect the values of radium equivalent which is used in the context of radiation protection to express the combined activity from all radioactive elements present in a material study area.

$$Ra_{eq} = 0.12^{232}\text{K} + 180.58 \qquad (16)$$

Where the values of slope and intercept are 0.12 and 180.58 Bq kg^{-1} respectively as shown in Eq. (16). From Figs. 4(a), 4(b) and 4(c) it is observed that there is a good correlation between the Ra_{eq} against ^{232}Th in comparison to the correlation between Ra_{eq} and ^{238}U, ^{40}K. Figures 5(a), 5(b) and 5(c) show the relation of absorbed dose rate measurement which quantifies the amount of ionizing radiation absorbed by a unit mass of material over a an hour. These indicatethe correlation between absorbed dose rate in nSv hr^{-1} and ^{238}U, ^{232}Th and ^{40}K activity concentrations in Bq kg^{-1}. We obtained Pearson correlation coefficient between ^{232}Th concentration and absorbed dose rate (r = 0.68), whereas that of with ^{238}U and ^{40}K are 0.45 and 0.58 respectively. From three plots, we can conclude that a major portion ofthe dose was contributed by ^{232}Th activity concentration in comparison to activity concentration of ^{238}U and ^{40}K (Rangaswamy *et al.*, 2016). From above it is also noticed that it exceeds the recommended dose limit.

Figure 6(a) express the ^{238}U activity concentration map of the surveyed mining area. We obtained maximum value (295.87 Bq kg^{-1}) nearly 8.5 times the world average value (33 Bq kg^{-1}) whereas the minimum value is nearly 1/10 of that value. Here color coding and symbol mentioned as red (diamond), yellow (circle), blue (triangle), and black (radiation symbol) for several concentration ranges as shown in Figs. 6(a), 6(b), 6(c) and 6(d) as activity and dose rate distribution maps respectively. Figure 6(b) denotes the map of activity concentrations of ^{232}Th in Bq kg^{-1} at the surveyed mining areas of Lalitpur district.

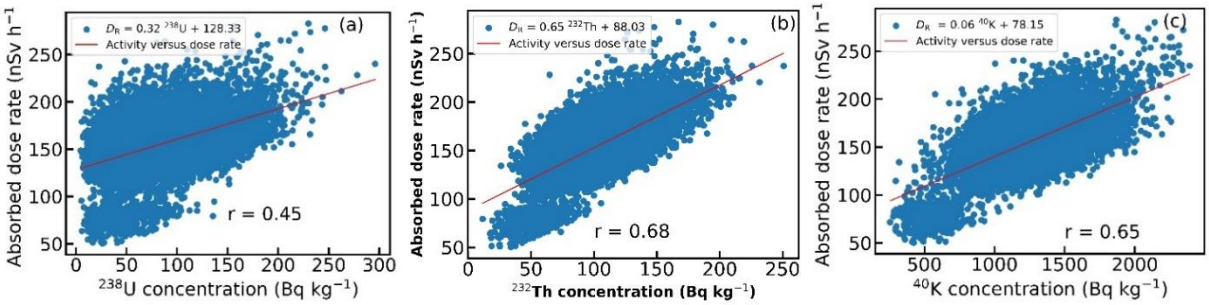

Figure 5. Correlation between activity concentration of ^{238}U (a), ^{232}Th (b), and ^{40}K (c) with dose rate

Table 3. Matrix showcasing the Pearson correlations among the variables

Variables	^{238}U	^{232}Th	^{40}K	R_{eq}	D_R	$AEDE_O$	$AEDR_I$	$ELCR_O$	$ELCR_I$	AGDE	H_{in}	H_{ex}	I_γ	I_α	RLI	AUI
^{238}U	1.00	-0.21	-0.03	0.49	0.45	0.45	0.45	0.45	0.45	0.52	0.79	0.49	0.44	1.00	0.44	0.63
^{232}Th	-0.21	1.00	0.34	0.68	0.68	0.68	0.68	0.68	0.68	0.66	0.38	0.68	0.69	-0.21	0.69	0.63
^{40}K -	0.03	0.34	1.00	0.58	0.65	0.65	0.65	0.65	0.65	0.56	0.39	0.58	0.65	-0.03	0.65	0.29
R_{eq}	0.49	0.68	0.58	1.00	0.99	0.99	0.99	0.99	0.99	0.99	0.92	1.00	0.99	0.487	0.99	0.95
D_R	0.45	0.68	0.65	0.99	1.00	1.00	1.00	1.00	1.00	0.99	0.90	0.99	1.00	0.45	1.00	0.92
$AEDR_O$	0.45	0.68	0.65	0.99	1.00	1.00	1.00	1.00	1.00	0.99	0.90	0.99	1.00	0.45	1.00	0.92
$AEDR_I$	0.45	0.68	0.65	0.99	1.00	1.00	1.00	1.00	1.00	0.99	0.90	0.99	1.00	0.45	1.00	0.92
$ELCR_O$	0.45	0.67	0.65	0.99	1.00	1.00	1.00	1.00	1.00	0.99	0.90	0.99	1.00	0.45	1.00	0.92
$ELCR_I$	0.45	0.68	0.65	0.99	1.00	1.00	1.00	1.00	1.00	0.99	0.90	0.99	1.00	0.45	1.00	0.92
AGDE	0.52	0.66	0.56	0.99	0.99	0.99	0.99	0.99	0.99	1.00	0.93	0.99	0.99	0.52	0.99	0.96
H_{in}	0.79	0.38	0.39	0.92	0.90	0.90	0.90	0.90	0.90	0.93	1.00	0.92	0.89	0.79	0.89	0.94
H_{ex}	0.49	0.68	0.58	1.00	0.99	0.99	0.99	0.99	0.99	0.99	0.91	1.00	0.99	0.49	0.99	0.95
I_γ	0.44	0.69	0.65	0.99	1.00	1.00	1.00	1.00	1.00	0.99	0.89	0.99	1.00	0.44	1.00	0.92
I_a	1.00	-0.21	-0.03	0.49	0.45	0.45	0.45	0.45	0.45	0.52	0.79	0.49	0.44	1.00	0.45	0.63
RLI	0.44	0.69	0.65	0.99	1.00	1.00	1.00	1.00	1.00	0.99	0.89	0.99	1.00	0.436	1.00	0.92
AUI	0.63	0.63	0.29	0.95	0.92	0.92	0.92	0.92	0.92	0.96	0.94	0.95	0.92	0.63	0.92	1.00

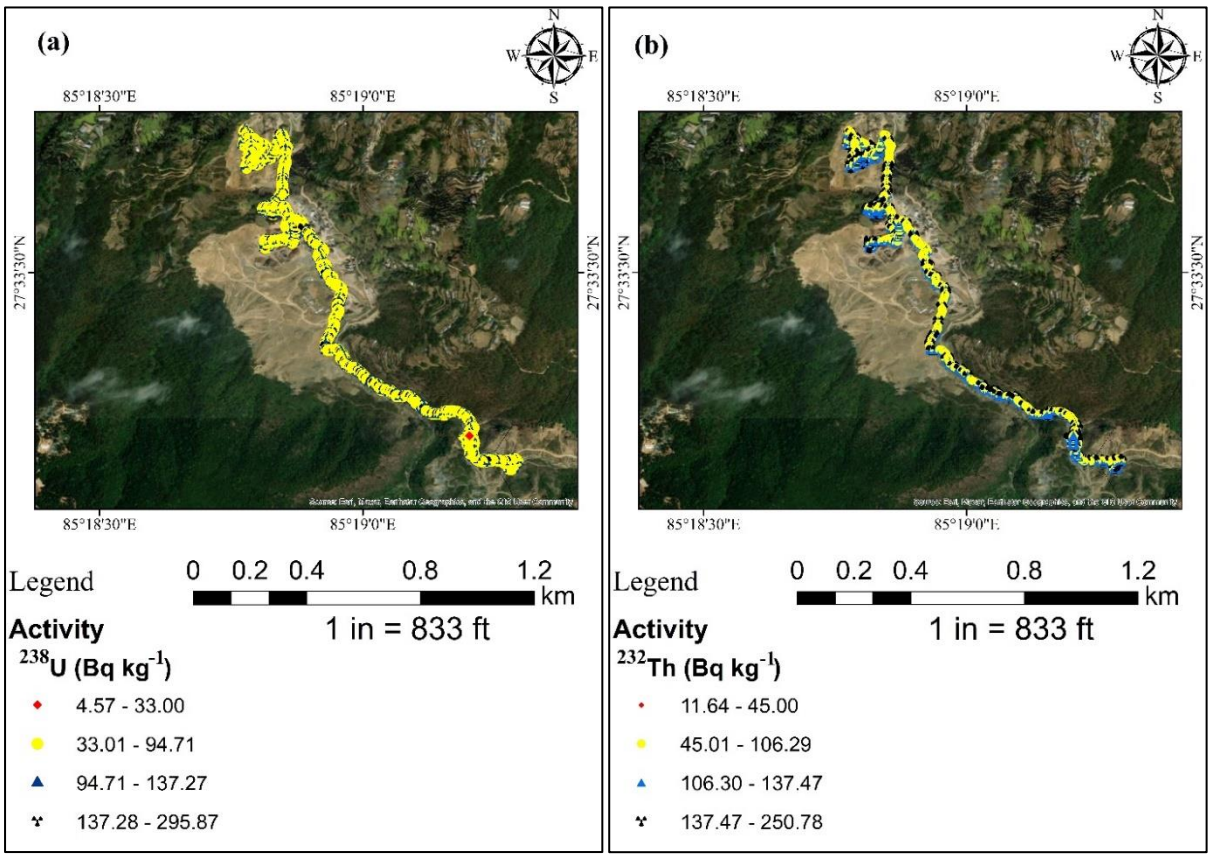

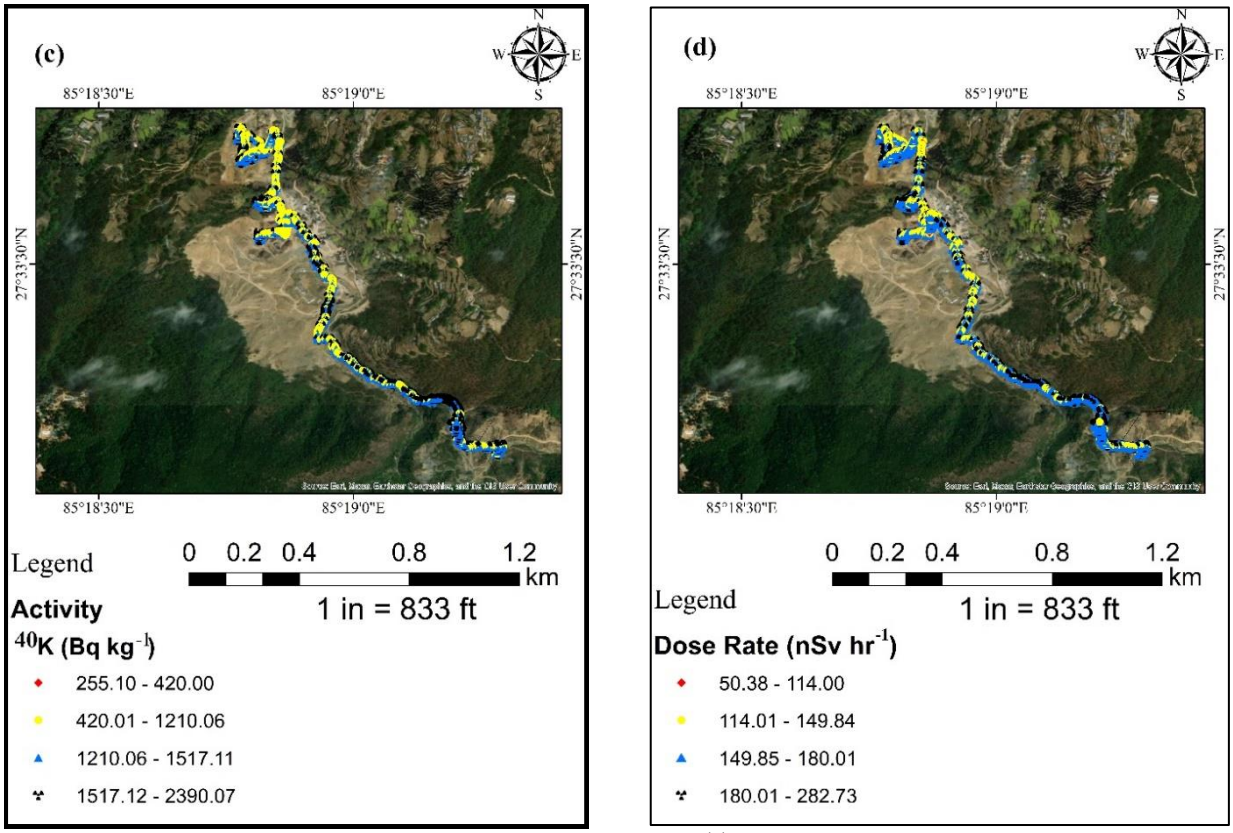

Figure 6. Distribution of activity concentration of (a) ^{238}U, (b) ^{232}Th, (c) ^{40}K and (d) Gamma dose rate (nSv hr^{-1}) mapping of study region with base map at mining area South Lalitpur

Table 4. Comparison of activity concentration and hazard indices with different parts of the world

Particulars	*A*U Bq kg^{-1} $\times10^{-3}$	*A*th Bq kg^{-1} $\times10^{-3}$	*A*K Bq kg^{-1}	Raeq Bq kg^{-1}	*D*R nSv hr^{-1}	*AEDR*O mSv y^{-1}	*AEDR* mSv y^{-1}	*ELCR*O $\times10^{-3}$	References
Poland	-	-	-	-	-	0.52	-	-	(Tchorz-Trzeciakiewicz *et al.*, 2023)
Nepal	108.41± 29.66	102.06± 28.25	1082.35±251.03		152.32± 15.07		-	-	(Mishra and Khanal, 2023b)
Nigeria	-	64.89 ± 1.50	181.38± 2.22	134.97	61.68	0.076	-	-	(Adewoyin *et al.*, 2022)
Nigeria	35.44 ± 0.97	92.57 ± 1.17	137.59 ± 2.42	202.15	84.770 ± 0.97	0.078	-	-	(Joel *et al.*, 2021)
Korea	63.1 ± 1.3	99.2 ± 1.5	1060 ± 14	-		125 ± 6	-	-	(Hassan *et al.*, 2018)
Kenya	240±17	626 ±27	401±21	-	408±20	2.37±0.09	-	-	(Kaniu *et al.*, 2018a)
South Africa	-	64	390	-	-	0.078	-	-	(Bezuidenhout, 2015)
Egypt	947	64	33.2	499.0 - 3484.9	149.5 - 970	0.18 - 1.19	-	0.002 ± 0.001	(Gaafar *et al.*, 2021)
Turkey	1871 ±38	3467 ±9	309 ±2			2.04 ±0.03	4.08 ±0.05		(Yücel *et al.*, 2020)
Mining Area	85.82 ± 40.63	104.87 ± 30.42	1257.47 ± 304.37	332.62 ± 63.08	155.94 ± 29.09	0.19 ± 0.04	0.67 ± 0.12	0.67 ± 0.13	**Present Work**

Here we obtained a maximum value nearly 5.5 times the world average activity concentration of ^{232}Th (45 Bq kg^{-1}) whereas the minimum value is less than one fourth of that limit. Figure 6(c) shows the map of activity concentration of ^{40}K observed at the surveyed mining areas of the Lalitpur district. Here we obtained a maximum value (2390.07 Bq kg^{-1}) nearly more than 6.5 times the world average value of that concentration (420 Bq kg^{-1}) whereas the minimum

value 0.607 times that reported value (UNSCEAR, 2000). Fig. 6 (d) shows the gamma dose rate maps for the surveyed mining areas of Lalitpur district. Here we obtained a maximum value of up to 2.5 times the general public dose rate limit (1 mSv $y^{-1} \cong 114$ nSv hr^{-1}) whereas minimum value less than 50% of that limit. Table 3 shows Pearson correlation coefficients between the radioactive concentrations and hazard indices around the mining area. From observed data, it has been observed that there is a negative correlation between ^{238}U and (^{232}Th , ^{40}K) activity concentrations whereas (^{232}Th and ^{40}K) has a positive correlation. However, the rest radiological parameters have a very good correlation with the activity concentrations of NORMs. Observed radiological concentrations and hazard indices compared with published work with several countries as mentioned in Tables 4 and 5. From this comparison, we observed that most of the parameters are above the world average mentioned in the UNSCEAR report (UNSCEAR, 2000).

Table 5. Comparison of hazard indices with different part of world

Particulars	*ELCR*I 10^{-3}	AGDE μSv hr^{-1}	H_{in}	H_{ex}	I_γ	I_a	RLI	AUI	References
Poland	-	-	-	-	-	-	-	-	(Tchorz-Trzeciakiewicz *et al.*, 2023)
Nepal	-	-	-	-	-	-	-	-	(Mishra & Khanal, 2023b)
Nigeria	-	-	-	0.36	-	-	-	-	(Adewoyin *et al.*, 2022)
Nigeria	-	-	0.671	0.275	-	-	-	-	(Joel *et al.*, 2021)
Korea	-	-	-	-	-	-	-	-	(Hassan *et al.*, 2018)
Kenya	-	-	-	-	-	-	-	-	(Kaniu *et al.*, 2018a)
South Africa	-	-	-	-	-	-	-	-	(Bezuidenhout, 2015)
Egypt	-	-	2.58 - 18.69	1.35 - 9.42	-	-	-	-	(Bezuidenhout, 2015)
Turkey	-	-	22.9 ± 0.4	18.2 ± 0.3	-	-	-	-	(Yücel *et al.*, 2020)
Mining Area	2.34 ± 0.44	972.67 ± 185.88	1.13 ± 0.24	0.90 ± 0.17	1.23 ± 0.23	0.43 ± 0.20	2.46 ± 0.46	2.17 ± 0.47	Present work
UNSCEAR	0.903	0.30	1	1	1	1	1	2	(UNSCEAR, 2000)

CONCLUSIONS

This study aimed to investigate the concentrations of naturally occurring radioactive nuclei and associated hazard indices in the mining area of Lalitpur district, near the capital city of Nepal, utilizing in-situ portable gamma-ray spectrometry. The radiological concentrations in the study region were found to be significantly elevated compared to the worldwide average. The mean concentrations of ^{238}U, ^{232}Th, and ^{40}K were measured at 85.82 Bq kg^{-1} ± 40.63 Bq kg^{-1}, 104.87 Bq kg^{-1} ± 30.42 Bq kg^{-1}, and 1257.47 ± 304.37 Bq kg^{-1}, respectively. The assessment of various hazard indices revealed the following average values:

- Radium equivalent index (Ra_{eq}): 332.62 ± 63.08 Bq kg^{-1}
- Absorbed dose rate (D_R): 155.94 ± 29.09 nSv hr^{-1}
- Outdoor annual effective dose equivalent ($AEDR_O$): 0.19 ± 0.04 mSv yr^{-1}
- Indoor annual effective dose equivalent ($AEDR_I$): 0.67 ± 0.13 mSv yr^{-1}
- Outdoor excess lifetime cancer risk ($ELCR_O$): 0.67 ± 0.13

Despite the elevated radionuclide concentrations, the mean radium equivalent activity in the study area was found tobe below the recommended safe limit of 370 Bq kg^{-1}. However, the average dose rate exceeded twice the worldwide average values, measuring at 155.94 ±29.09 nSv hr^{-1}. On a positive note, the outdoor and indoor average effective dose values were lower than the safety limit (1 mSv yr^{-1}) proposed in the UNSCEAR report. The multivariate descriptive statistical analysis revealed skewness values within the range of -1 <skewness <1, covering approximately 68.27% of the data distribution. Positive kurtosis values (>0) for all parameters indicated a leptokurtic distribution. This study highlights the need for further experimental investigations of construction materials in the mining region to better understand and evaluate the potential exposure of the public and the potential impact after using such materials in construction applications. The elevated levels of radionuclides and associated hazard indices in mining areas underscore the importance of rigorous monitoring and safety measures in these regio

ACKNOWLEDGEMENTS

D. R. Upadhyay acknowledges the University Grants Commission, Nepal, for the PhD Fellowship and Research Support Fund (award number PhD-78/79-S&T-14). D. R. Upadhyay, P. Adhikari, B. V. Khatri, and R. Khanal acknowledge the support from the International Atomic Energy Agency, Austria (IAEA, TC Project NEP0002) for support in establishing a Nuclear Laboratory with computational facilities. The Ministry of Education, Science and Technology, Government of Nepal, is acknowledged for coordination with IAEA. The Geographic Information Infrastructure Division, Survey Department, Government of Nepal, is acknowledged for providing the necessary maps of different levels. The Department of Mines and Geology, Government of Nepal, is acknowledged for granting permission for fieldwork.

AUTHOR CONTRIBUTIONS

D. R. Upadhyay: Conceptualization, field survey, methodology, validation, data analysis, visualization, writing original draft; P. Adhikari: field survey, and data analysis; B. V. Khatri: field survey, review and editing; S. M. Tajudin: writing, review and editing; H. Kalakhety: writing, review and editing; R. Khanal: methodology, resources, writing, review, validation, visualization, supervision, and editing.

CONFLICT OF INTEREST

No conflicts of interest exist in relation to the research work presented in this study.

DATA AVAILABILITY STATEMENT

Data will be made available on request with a suitable reason.

REFERENCES

Adewoyin, O., Maxwell, O., Akinwumi, S., Adagunodo, T., Embong, Z., & Saeed, M. (2022). Estimation of activity concentrations of radionuclides and their hazard indices in coastal plain sand region of Ogun state. *Scientific Reports*, 12(1), 1–8. https://doi.org/10.1038/s41598-022-06064-3

Attallah, M. F., Abdelbary, H. M., Elsofany, E. A., Mohamed, Y. T., & Abo-Aly, M. M. (2020). Radiation safety and environmental impact assessment of sludge TENORM waste produced from petroleum industry in Egypt. *Process Safety and Environmental Protection*, 142, 308–316.https://doi.org/10.1016/j.psep.2020.06.012

Belyaeva, O., Movsisyan, N., Pyuskyulyan, K., Sahakyan, L., Tepanosyan, G., & Saghatelyan, A. (2021). Yerevan soil radioactivity: Radiological and geochemical assessment. *Chemosphere*, 265, 129173. https://doi.org/10.1016/j.chemosphere.2020.129173

Bezuidenhout, J. (2015). In situ gamma ray measurements of radionuclides at a disused phosphate mine on the West Coast of South Africa. *Journal of Environmental Radioactivity*, 150, 1–8. https://doi.org/10.1016/j.jenvrad.2015.07.030

Gaafar, I., Hanfi, M., El-Ahll, L. S., & Zeidan, I. (2021). Assessment of radiation hazards from phosphate rocks, Sibaiya area, central eastern desert, Egypt. *Applied Radiation and Isotopes*, 173, 109734. https://doi.org/10.1016/j.apradiso.2021.109734

Galbiati, C., Pocar, A., Franco, D., Ianni, A., Cadonati, L., & Schönert, S. (2005). Cosmogenic C^{11} production and sensitivity of organic scintillator detectors to pep and CNO neutrinos. *Physical Review C*, 71(5), 055805. https://doi.org/10.1103/PhysRevC.71.055805

García-León, M. (2023). *Detecting Environmental Radioactivity*. Springer Nature. https://doi.org/10.1007/978-3-031-09970-0

Ghias, S., Satti, K. H., Khan, M., Dilband, M., Naseem, A., Jabbar, A., Kali, S., Ur-Rehman, T., Nawab, J., Aqeel, M., et al. (2021). Health risk assessment of radioactive footprints of the urban soils in the residents of Dera Ghazi Khan, Pakistan. *Chemosphere*, 267, 129171. https://doi.org/10.1016/j.chemosphere.2020.129171

Hassan, N., Kim, Y., Jang, J., Chang, B., & Chae, J. (2018). Comparative study of precise measurements of natural radionuclides and radiation dose using in-situ and laboratory γ-ray spectroscopy techniques. *Scientific Reports*, 8(1), 14115. https://doi.org/10.1038/s41598-018-32220-9

ICRP (1991). 1990 Recommendations of the International Commission on Radiological Protection. ICRP Publication 60. *Annals ICRP*, 21, 1–3.

Inoue, K., Fukushi, M., Van Le, T., Tsuruoka, H., Kasahara, S., & Nimelan, V. (2020). Distribution of gamma radiation dose rate related with natural radionuclides in all of Vietnam and radiological risk assessment of the built-up environment. *Scientific Reports*, 10(1), 1–14. https://doi.org/10.1038/s41598-020-69003-0

Joel, E., Maxwell, O., Adewoyin, O., Olawole, O., Arijaje, T., Embong, Z., & Saeed, M. (2019). Investigation of natural environmental radioactivity concentration in soil of coastaline area of Ado-Odo/Ota Nigeria and its radiological implications. *Scientific Reports*, 9(1), 1–8. https://doi.org/10.1038/s41598-019-40884-0

Joel, E., Omeje, M., Olawole, O., Adeyemi, G., Akinpelu, A., Embong, Z., & Saeed, M. (2021). In-situ assessment of natural terrestrial-radioactivity from Uranium-238 (^{238}U), Thorium-232 (^{232}Th) and Potassium-40 (^{40}K) in coastal urban-environment and its possible health implications. *Scientific Reports*, 11(1), 1–14. https://doi.org/10.1038/s41598-021-96516-z

Kaniu, M., Angeyo, H., Darby, I., & Muia, L. (2018a). Rapid in-situ radiometric assessment of the Mrima Kiruku high background radiation anomaly complex of Kenya. *Journal of Environmental Radioactivity*, 188, 47–57. https://doi.org/10.1016/j.jenvrad.2017.10.014

Kaniu, M., Angeyo, K., & Darby, I. (2018b). Occurrence and multivariate exploratory analysis of the natural radioactivity anomaly in the south coastal region of Kenya. *Radiation Physics and Chemistry*, 146, 34–41. https://doi.org/10.1016/j.radphyschem.2018.01.009

Kaniu, M., Darby, I., & Angeyo, H. (2019). Assessment and mapping of the high background radiation anomaly associated with laterite utilization in the south coastal region of Kenya. *Journal of African Earth Sciences*, 160, 103606. https://doi.org/10.1016/j.jafrearsci.2019.103606

Khadka, D. R. & Lamsal, M. (2020). Geology and Ground Radiometric Survey for U/Th Prospecting and Radiation Hazard Mapping in Parts of Shivpuri Area, Northern Part of Kathmandu Valley. *Annual Report of Department of Mines and Geology*, 12, 31–37. https://dmgnepal.gov.np/uploads/documents/annual-report-dmg-no-12pdf-2114-352-1687930459.pdf

Khadka, D. R. & Lamsal, M. (2022). Geology and Mineral Prospection Using Gamma Ray Spectrometer in Parts of Gorkha District, Nepal. *Annual Report of Department of Mines and Geology*, 13, 93–103. https://dmgnepal.gov.np/uploads/documents/annual-report-13pdf-1518-759-1688108600.pdf

Khadka, D. R. & Maharjan, N. (2019). Status of Uranium and Thorium Prospects in Nepal. *Annual Report of Department of Mines and Geology*, 11, 31–37. https://dmgnepal.gov.np/uploads/documents/dmg-annual-report-11pdf-3031-305-1687762559.pdf

Liu, X. & Lin, W. (2018). Natural radioactivity in the beach sand and soil along the coastline of Guangxi Province, China. *Marine Pollution Bulletin*, 135, 446–450. https://doi.org/10.1016/j.envpol.2017.12.095

Mishra, A. & Khanal, R. (2019). Outdoor effective dose and associated health risk in the premises of Tribhuvan University in-situ gamma ray spectrometry. *Himalayan Physics*, 8, 47–52. https://doi.org/10.3126/hp.v8i0.30001

Mishra, A. & Khanal, R. (2023a). Assessment of ^{137}Cs in the Environment of Hetauda City, Nepal by In-Situ Gamma Ray Spectrometry. *Atom Indonesia*, 49(2), 109–113. https://doi.org/10.55981/aij.2023.1268

Mishra, A. & Khanal, R. (2023b). In-situ Radiometric Assessment of UNESCO World Heritage Sites in Kathmandu Valley of Nepal Using Gamma Ray Spectrometry. *Jordan Journal of Physics*, 16(2), 215–227. https://doi.org/10.47011/16.2.9

Orosun, M., Ajibola, T., Akinyose, F., Osanyinlusi, O., Afolayan, O., & Mahmud, M. (2021). Assessment of ambient gamma radiation dose and annual effective dose associated with radon in drinking water from gold and lead mining area of Moro, North-Central Nigeria. *Journal of Radioanalytical and Nuclear Chemistry*, 328, 129–136. https://doi.org/10.1007/s10967-021-07644-9

Pfützner, M., Karny, M., Grigorenko, L., & Riisager, K. (2012). Radioactive decays at limits of nuclear stability. *Reviews of Modern Physics*, 84(2), 567. https://doi.org/10.1103/RevModPhys.84.567

Rangaswamy, D., Srilatha, M., Ningappa, C., Srinivasa, E., & Sannappa, J. (2016). Measurement of natural radioactivity and radiation hazards assessment in rock samples of Ramanagara and Tumkur districts, Karnataka, India. *Environmental Earth Sciences*, 75, 1–11. https://doi.org/10.1007/s12665-015-5195-8

Ravisankar, R., Chandrasekaran, A., Vijayagopal, P., Venkatraman, B., Senthilkumar, G., Eswaran, P., & Rajalakshmi, A. (2012). Natural radioactivity in soil samples of Yelagiri Hills, Tamil Nadu, India and the associated radiation hazards. *Radiation Physics and Chemistry*, 81(12), 1789–1795. https://doi.org/10.1016/j.radphyschem.2012.07.003

Ravisankar, R., Vanasundari, K., Suganya, M., Raghu, Y., Rajalakshmi, A., Chandrasekaran, A., Sivakumar, S., Chandramohan, J., Vijayagopal, P., & Venkatraman, B. (2014). Multivariate statistical analysis of radiological data of building materials used in Tiruvannamalai, Tamilnadu, India. *Applied Radiation and Isotopes*, 85, 114–127. https://doi.org/10.1016/j.apradiso.2013.12.005

Sam, A. & Abbas, N. (2001). Assessment of radioactivity and the associated hazards in local and imported cement types used in Sudan. *Radiation Protection Dosimetry*, 93(3), 275–277. https://doi.org/10.1093/oxfordjournals.rpd.a006440

Suresh, S., Rangaswamy, D., Sannappa, J., Dongre, S., Srinivasa, E., & Rajesh, S. (2022). Estimation of natural radioactivity and assessment of radiation hazard indices in soil samples of Uttara Kannada district, Karnataka, India. *Journal of Radioanalytical and Nuclear Chemistry*, 331(4), 1869–1879. https://doi.org/10.1007/s10967-021-08145-5

Tchorz-Trzeciakiewicz, D., Kozłowska, B., & Walencik-Łata, A. (2023). Seasonal variations of terrestrial gamma dose, natural radionuclides and human health. *Chemosphere*, 310, 136908. https://doi.org/10.1016/j.chemosphere.2022.136908

UNSCEAR (2000). *Sources and Effects of Ionizing Radiation, United Nations Scientific Committee on the Effects of Atomic Radiation (UNSCEAR) 2000 Report, Volume I: Report to the General Assembly, with Scientific Annexes-Sources*. United Nations. https://doi.org/10.18356/170c70d9-en

Usikalu, M. R., Orosun, M. M., Akinpelu, A., & Oyewumi, K. J. (2022). A study of environmental radioactivity measurement of selected Kaolin mining fields in Kwara, Nigeria. *Cogent Engineering*, 9(1), 2105034. https://doi.org/10.1080/23311916.2022.2105034

Yücel, H., Övüç, S., Akkaya, G., & Çakmak, S¸ . (2020). Estimation of Radiological Exposure Levels in a Mining Area Based on ^{238}U, ^{226}Ra, ^{232}Th and ^{40}K Activity Measurements: A Case Study for Beylikova Sivrihisar Complex Ore Site in Turkey. *Radiation Protection Dosimetry*, 190(3), 297–306. https://doi.org/10.1093/rpd/ncaa104